Fuel 268 (2020) 117334

Contents lists available at ScienceDirect

Fuel

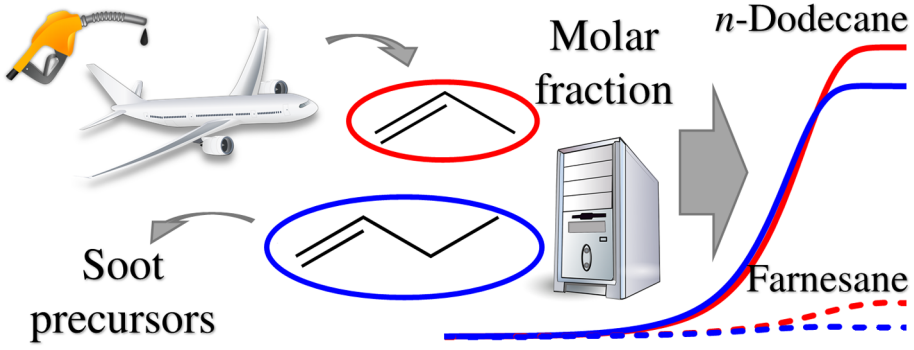
journal homepage: www.elsevier.com/locate/fuel

Soot precursors in farnesane and *n*-dodecane decomposition: A computational approach

Marcelo André Petry Pontes[a], Francisco Bolivar Correto Machado[a], Orlando Roberto-Neto[b], Luiz Fernando de Araujo Ferrão[a,*]

[a] Departamento de Química, Instituto Tecnológico de Aeronáutica, 12228-900 São José dos Campos, SP, Brazil
[b] Divisão de Aerotermodinâmica e Hipersônica, Instituto de Estudos Avançados, 12228-840 São José dos Campos, SP, Brazil

GRAPHICAL ABSTRACT



ARTICLE INFO

Keywords:
Hydrogen abstraction
β-scission reaction
Density functional theory
Transition state theory
2,6,10-Trimethyldodecane

ABSTRACT

The worldwide increase concern about the use of fossil fuels is causing a running for the development of green fuels, trying to slow down the emissions of soot and greenhouse gases. Recent studies are pointing up that branched carbon chain structures of alkanes, terpenoids, and sesquiterpenes produce less soot during combustion, they have been employed as an additive in diesel/kerosene engines. In this work, a decomposition sub-mechanism of farnesane and *n*-dodecane fuels was studied, using the calculated Arrhenius parameters for several hydrogen abstractions and β-scission elementary reactions to compare the preceding species of the soot precursors. The calculations were carried out using density functional theory to obtain the thermochemical properties of all molecules and transition state theory to calculate the thermal rate coefficients. The results showed the importance of the thermochemical analysis in choosing the appropriate temperature range for the selected reactions, to obtain a qualitatively appropriate set of kinetic parameters. The molar fraction comparison resulting from the sub-mechanism of the two fuels revealed that farnesane yields a smaller amount of species necessary to produce soot precursors due to the position of the branched carbons. The methodology used here allows the construction of additive mechanisms and can be used to aid the design of new fuels that could be more efficient and/or less polluting. By investigating, for example, the first steps of a fuel decomposition in a reduced mechanism, avoiding the complexity of a complete mechanism, while also generating fairly accurate kinetic parameters for elementary reactions.

* Corresponding author.
E-mail address: ferrao@ita.br (L.F.d.A. Ferrão).

https://doi.org/10.1016/j.fuel.2020.117334
Received 30 October 2019; Received in revised form 18 January 2020; Accepted 4 February 2020
Available online 17 February 2020
0016-2361/ © 2020 Elsevier Ltd. All rights reserved.

1. Introduction

There has been an increased concern on soot growth reactions from soot precursor molecules, such as polycyclic aromatic hydrocarbons (PAHs). Although PAHs are difficult to estimate because of their short atmospheric lifetime, causing variations in their concentration, which are strongly dependent on time and location of their emissions, soot emitted into the atmosphere is associated to some degree with atmospheric warming. In any case, the emission of these particles could be avoided by changing the combustion reaction mechanism, either by directly modifying combustion parameters or by changing the structure of the starting fuel [1]. Recent experimental and computational studies describe the reactions and processes involved in the formation of PAHs and their role in the generation of soot precursors [2–10].

The flame studies were delimited in conditions of soot precursor reactions. Ruwe *et al.* [2,3] have studied the C_5 species (structures with 5 carbons) trends to form PAHs, obtaining the following order of importance: *n*-pentane < 1-pentene < 2-methyl-2-butene. While the alkane (*n*-pentane) had a higher amount of C_2 and C_3 species, the branched alkene (2-methyl-2-butene) had higher aromatics production, such as toluene, which contributes to the initiation of the PAHs formation mechanism. Tang *et al.* [4] observed in ethylene, propane, and ethylene/toluene flames that the increase of the C/H ratio of the fuel boosts the soot formation and also suggested that the soot nucleation reaction for these flames is prohibited in either low or high temperatures. At lower temperatures (T_{max} = 1586 K) the rate of nucleation is slow, meanwhile, at higher temperatures (T_{max} = 2131 K) the thermodynamical reversibility of PAHs formation is more important than soot formation reactions. Banerjee *et al.* [5] compared some chemical kinetic models that diverged among themselves in predictions of the molar fraction for intermediate and product species, *e.g.* ethene, propene, and but-1-ene, where they have optimized the model with *n*-dodecane pyrolysis and oxidation obtained in a flow reactor. Kathrotia *et al.* [6] have investigated the $C_2 + C_4$ route as the major route of benzene formation from *n*-hexane, *n*-nonane and *n*-dodecane molecules at intermediate flame temperatures (<1200 K). A detailed model was reproduced in agreement with the experiment, which provides an important contribution to the prediction of soot precursors, although future studies of other fuel classes are still needed. In n-dodecane flames, Wang *et al.* [7] found that benzene formation comes from $C_2H_x + C_4H_y$ (~76%) and $C_3H_3 + C_3H_3$ (~18%) routes.

Computational studies have also contributed to the analysis of soot formation. Han *et al.* [8,9] have simulated the initial steps of soot nanoparticles formation and the initial reactivity models of fuel pyrolysis by reactive molecular dynamics (ReaxFF) for a rocket propellant (RP-1). It was shown that soot particle size increases at higher pressure conditions and under intermediate conditions of temperature and equivalent ratio and the pyrolysis depends on the number of species used, especially when branched molecules are taken into account [8]. However, both 3-component surrogate model and 24-component model for RP-1 fuel pyrolysis have a behavior similar to normal alkanes [9]. Ashraf *et al.* [10] also studied the pyrolysis of *n*-dodecane and jet-propulsion fuel (JP-10) with toluene mixtures using the ReaxFF technique concluding that the *n*-dodecane mixture generates larger radical pools than JP-10 mixtures, and these radicals react with toluene molecules more quickly.

There has been an increase in the research of soot emission of biofuels [1,11–16], given the future scarcity of fossil fuels and increased pollutant emissions in the atmosphere. The International Air Transport Association (IATA) has taken a major initiative to reduce pollutant emissions since the aviation industry is responsible for 2 to 3% of global CO_2 emissions [16]. The main goals of IATA are to achieve carbon-neutral growth starting in 2020 and a 50% cut in 2005-level carbon emissions by 2050. To reach these recommended concentration levels, the aviation industry is developing new sustainable aviation fuels which could reduce carbon emissions per passenger by up to 80% compared to the 1960s [17,16]. New specification standards and test methods covering the manufacture of blends between conventional and synthetic fuels for use in aviation engines were also issued [18,19].

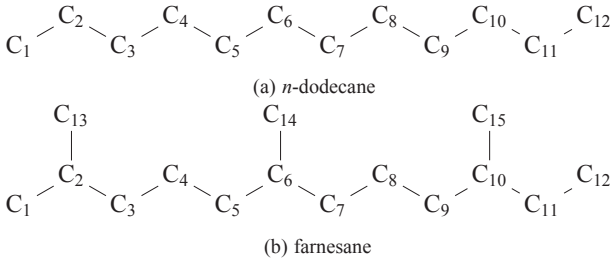
Advanced biofuels can be obtained using biochemical processes to produce longer-chain alcohols, fatty acids, alkanes and alkenes from biomass feedstock [13–15]. One class of hydrocarbons that has great potential to serve as advanced biofuels is the isoprenoids (also called terpenoids), which are built by units with five branched carbons [13,14]. Although the inclusion of tertiary carbons decreases the combustion quality for diesel engines (the cetane number), the presence of a few branches disrupts the stacking of the carbon chains and consequently decreases the freezing point, which is important for jet fuel applications [13]. The sesquiterpene class is formed by three isoprene units (15 carbon atoms) and it has shown to be promising biofuels for aerospace applications [20,21]. In particular, the sesquiterpene compound called farnesene (3,7,11-trimethyl-1,3,6,10-dodecatetraene, $C_{15}H_{24}$) is derived from fermentation of sugars and its hydrogenation produces the farnesane molecule (2,6,10-trimethyldodecane, $C_{15}H_{32}$) [22,23]. Farnesane is one of the most promising advanced biofuels for commercialization as a fuel blend for aviation and diesel engines [24–27], due to the smaller amount of nitrogen oxides and soot produced in its combustion [28,29].

Previous studies involving farnesane biofuel were made considering the thermal stability of its mixture with kerosene rocket propellant [21], its ignition delay time and thermal decomposition [24–27], and its performance and emission on diesel engines [28]. More recently, the first quantitative speciation data of the combustion [29] and the first reaction mechanism obtained from experimental data coupled with the modeling study of global the combustion [30] were obtained.

The quantitative speciation data obtained by Oßwald *et al.* [29] shows the hydrogen abstraction (H-abstraction) and subsequent β-scission reactions of C–H or C–C bond as possible fuel decomposition pathways, as well as an analysis of the PAHs formation for farnesane combustion. It was observed that the methyl and ethyl group elimination and the formation of a double carbon bond from β-scission of carbon-6 alkyl were favored. Ignition delay time and laminar burning velocity were obtained by Richter *et al.* [30] to compare farnesane and Jet A-1 combustion. A reaction model for farnesane combustion was also developed, considering a reaction mechanism involving several intermediary species to find out the global combustion properties.

The detailed understanding of the combustion chemistry is challenging and involves numerous reactions and intermediary species that depend on the molecular composition of the fuel. The knowledge of these processes is one of the key points to understand how the concentration of soot precursors produced can be reduced in the combustion processes. Fuel decomposition involves elementary reactions that contain several processes of dissociation and formation of many molecules. However, the first elementary reactions are fundamental to the knowledge about the formation of soot precursors. Within this group, there are H-abstraction, β-scission, C–C break and C–H as the main initial reactions in alkane decompositions. Laminar flame speeds of the *n*-dodecane calculated by Ji *et al.* [31] showed that 90% of fuel consumption was through H-abstraction of the molecule, in which 67% was taken by a hydrogen atom.

From the computational quantum chemistry perspective, the design of a fuel which produces low soot would formally require the complete knowledge of the electronic energy surfaces of all elementary reactions within the combustion mechanism. However, this is unfeasible for fuel molecules containing more than a couple of atoms since the number of reaction pathways and, therefore, the number of elementary reactions, rapidly increases with the size of the molecule. The alternative is to use a reduced mechanism or even to focus on a small set of elementary reactions, which are expected to play a central role in determining the concentration of certain species. The current challenge is to predict the kinetic parameters of these reactions from thermochemical calculations within or close to the chemical accuracy (~1 kcal mol^{-1}) [32]. Previous



(a) *n*-dodecane

(b) farnesane

Fig. 1. Chemical representation and the labels used for the whole of this work of the studied molecules. The hydrogen atoms are implicit.

works have focused on an experimental and theoretical approach to obtain the Arrhenius parameters of the H-abstraction [33–39] and β-scission [35,36,40–42] elementary reactions for alkane molecules, which are used in hydrocarbon reaction models [43,44,38,30,6,39]. In this work density functional theory (DFT) and the transition state theory (TST) were used to compare both thermodynamic and kinetic properties of some elementary reactions involved in the first steps of the farnesane and *n*-dodecane (Figs. 1a and 1b) thermal decomposition. In particular, DFT and TST were used to study several hydrogen abstraction reactions by a hydrogen atom and the subsequent β-scission reactions of farnesane and *n*-dodecane molecules. The main goal is to track down the lower soot formation of farnesane to these first decomposition steps and to verify if a standard molecular quantum chemistry methodology can identify these differences.

2. Methodology

2.1. Thermodynamics

A systematic study was carried out considering the initial fuel decomposition steps, as follows,

$$C_nH_{2n+2} + \cdot H \overset{\text{SP1}}{\rightleftharpoons} \cdot C_nH_{2n+1} + H_2 \tag{1}$$

$$\cdot C_nH_{2n+1} \overset{\text{SP2}}{\rightleftharpoons} \cdot C_mH_{2m+1} + C_{n-m}H_{2(n-m)} \tag{2}$$

in which Eq. (1) represents the reactants and products of all possible hydrogen abstractions of an alkane molecule ($\cdot C_nH_{2n+2}$) by a hydrogen atom, forming an alkyl radical ($\cdot C_nH_{2n+1}$) and a hydrogen molecule. The Eq. (2) shows the reactants and products of all possible β-scission reactions, where the alkyl radical produced in the previous step generates a smaller alkyl radical ($\cdot C_mH_{2\,m+1}$) and an alkene molecule ($C_{n-m}H_{2(n-m)}$). In this work, Eqs. (1) and (2) were calculated for *n*-dodecane ($n = 12$) and farnesane ($n = 15$) molecules.

The thermochemical properties of both reactions were obtained through the characterization of the stationary states (reactants, products and saddle points) through computational chemical methods, *i.e.*, by calculations of equilibrium geometries, harmonic vibrational frequencies to obtain the classical barrier height ($V^{\ddagger}$, electronic energy difference between the reactants and the saddle point), the adiabatic barrier height ($\Delta V_a^{G,\ddagger} = V^{\ddagger} + \Delta ZPE$), the electronic energy of the reaction ($\Delta_r E_0$) and the enthalpy of the reaction at 0 K ($\Delta_r H_0 = \Delta_r E_0 + \Delta ZPE$). The zero-point vibrational energies (ZPE) were calculated in the equilibrium geometry of each stationary state, as shown in Eq. (3), where h is the Planck constant, c is the speed of light and the $\tilde{\nu}_m$ is the frequency of a given *m*-vibrational mode. M is the total number of vibrational modes; for a non-linear system with n atoms, there are $3n - 6$ vibrational modes ($3n - 5$ if linear).

$$ZPE = \sum_{m}^{M} \frac{1}{2} hc\tilde{\nu}_m \tag{3}$$

Density functional theory (DFT) within M06-2X [45] functional approximation has been used to characterize the stationary states and to calculate their electronic energies and zero-point corrections, enabling the calculation of accurate thermochemical and kinetic parameters of each elementary reaction [46–50]. The geometry optimization of the stationary states was done in two steps. First, the cc-pVDZ basis set [51] was used to find the equilibrium geometries, especially in transition structures (saddle points). Subsequently, the maug-cc-pV(T + d)Z basis set [52] was used to obtain the final structures and energies. A frequency scale factor was used to correct the thermodynamic functions within the M06-2X/maug-cc-pV(T + d)Z model chemistry ($\lambda^{ZPE} = 0.971$) [53], empirically taking into account the anharmonicity of the vibrational modes. All these calculations were carried out using the Gaussian 09 program [54].

2.2. Kinetics treatment

Eqs. (1) and (2) can be combined and represented under a common set of variables as follows,

$$A + H \underset{k_{1r}^{i}}{\overset{k_{1f}^{i}}{\rightleftharpoons}} B_i + H_2 \underset{k_{2r}^{ij}}{\overset{k_{2f}^{ij}}{\rightleftharpoons}} C_{ij} + D_{ij} + H_2 \tag{4}$$

where, A is the alkane molecule, B and D are the alkyl radicals, C is the alkene molecule, k_{1f}^{i} and k_{1r}^{i} are the forward and reverse rate constants of H-abstraction reaction paths for each carbon alkyl formation ($i = 1, \ldots, n$), following the index of Fig. 1a and b. k_{2f}^{ij} and k_{2r}^{ij} are the forward and reverse rate constants of β-scission reaction paths considering the alkyl radicals produced previously ($i = 1, \ldots, n$) and $j = 1$, 2 or 3 depending of β-scission in the carbon chain.

The thermal rate constants ($k(T)$) were calculated considering the conventional TST model [55,32] (Eq. (5)),

$$k(T) = \sigma\kappa_{tun}(T)\frac{k_B T}{h}(c^{\circ})^{z}\exp\left(-\frac{\Delta^{\ddagger}G_T^{\circ}}{RT}\right) \tag{5}$$

where σ is a factor of symmetry that was set to one for the forward and reverse reactions, $\kappa_{tun}(T)$ is a transmission coefficient, k_B is Boltzmann's constant, h is Planck's constant, $\Delta^{\ddagger}G_T^{\circ}$ is the quasithermodynamic free energy of activation, R is the gas constant, c° is the standard state concentration, equal to RT/p°, where p° is the pressure at standard state and, the power factor z is 0 for unimolecular or 1 for bimolecular reactions.

The tunneling coefficient (κ_{tun}) was calculated with the Wigner tunneling correction factor [56], according to Eq. (6), where $\nu_i^{\ddagger}$ is the imaginary vibrational frequency of the saddle point related to the transition state of each reaction path.

$$\kappa_{tun} = 1 + \frac{1}{24}\left(\frac{h\nu_i^{\ddagger}}{k_B T}\right)^2 \tag{6}$$

The rate constants obtained with Eq. (5) for each reaction path involved in Eq. (4) were fitted from 800 K to 1200 K considering the three-parameter Arrhenius equation [57], as follows.

$$k(T) = AT^{b}\exp\left(-\frac{E_a}{RT}\right) \tag{7}$$

The fitted rate constants were used to describe the rate law of each elementary reaction, as shown in Eqs. (8)–(11),

$$r_{1f}\text{: } A + H \overset{k_{1f}^{i}}{\rightarrow} B_i + H_2 \tag{8}$$

$$r_{1r}\text{: } B_i + H_2 \overset{k_{1r}^{i}}{\rightarrow} A + H \tag{9}$$

$$r_{2f}\text{: } B_i \overset{k_{2f}^{ij}}{\rightarrow} C_{ij} + D_{ij} \tag{10}$$

$$r_{2r}\text{: } C_{ij} + D_{ij} \overset{k_{2r}^{ij}}{\rightarrow} B_i \tag{11}$$

and thus to obtain the concentration of each chemical species studied in

the mechanism presented in Eq. (4). The complete description of the mechanism is shown in Eqs. (12)–(15).

$$\frac{d[A]}{dt} = \frac{d[H]}{dt} = -\sum_{i=1}^{n} k_{1f}^{i}[A][H] + \sum_{i=1}^{n} k_{1r}^{i}[B_i][H_2] \tag{12}$$

$$\frac{d[H_2]}{dt} = \sum_{i=1}^{n} k_{1f}^{i}[A][H] - \sum_{i=1}^{n} k_{1r}^{i}[B_i][H_2] \tag{13}$$

$$\frac{d[B_i]}{dt} = k_{1f}^{i}[A][H] - k_{1r}^{i}[B_i][H_2] - \sum_{j=1}^{3} k_{2f}^{ij}[B_i] + \sum_{j=1}^{3} k_{2r}^{ij}[C_{ij}][D_{ij}] \tag{14}$$

$$\frac{d[C_{ij}]}{dt} = \frac{d[D_{ij}]}{dt} = \sum_{j=1}^{3} k_{2f}^{ij}[B_i] - \sum_{j=1}^{3} k_{2r}^{ij}[C_{ij}][D_{ij}] \tag{15}$$

This leads to a set of 82 and 29 coupled differential equations for farnesane and *n*-dodecane, respectively, which were solved numerically by using the backward differentiation formula (BDF) [58,59], as implemented in the Scilab 6.0.2 program [60]. The solutions of these equations, *i.e.*, the integrated rate laws, were used to obtain the concentration of several molecules over time. The Scilab script code written for this work is available in the Supplementary material. The initial concentration of farnesane, *n*-dodecane and hydrogen atom was 1 mol L^{-1}, while the concentration of all other species was considered zero. The results focus on the comparison of the concentration of 5 final products (ethene, propene, but-1-ene, methyl, and ethyl) which are directly related to the formation of soot precursors (especially propene), 10^{-2} s after the reaction mechanism started, and considering typical temperatures involved in fuel decompositions processes (from 800 K to 1200 K).

3. Results and discussion

The results are organized as follows: in Section 3.1, the thermochemical properties of the studied reactions are presented, including their energy profile and a discussion about the validity of the chosen subset of reactions in terms of the free energy involved in the molecule decomposition; the reaction rate of each elementary step is presented in Sections 3.2 (H-abstractions) and 3.3 (β-scissions), comparing the calculated values with those available in the literature; finally, in Section 3.4, the previously calculated elementary reactions are used in the chosen sub-mechanism to represent the initial steps of the fuel decomposition of farnesane and *n*-dodecane, and the differences in the concentration of key molecules that acts as soot precursors are discussed.

3.1. Thermochemistry properties

The energy diagrams of H-abstraction and β-scission, relative to the reactants ($C_{12}H_{26}$ + H and $C_{15}H_{32}$ + H), at 0 K, are presented in Figs. 2a and b, respectively. The H-abstraction shows three barrier height levels around 6 (only for farnesane), 8 and 11 kcal mol^{-1} in both molecules. These levels represent the abstraction occuring in tertiary (*t*-site), secondary (*s*-site) and primary carbons (*p*-site), respectively. The calculated enthalpy of reaction presented mean values in the order of −8, −7 and −4 kcal mol^{-1}, respectively.

The β-scission reactions have higher barriers compared to the H-abstraction. The barrier heights involved in the β-scission reactions of *n*-dodecane and farnesane were calculated in the range of 30–32 and 27–33 kcal mol^{-1}, respectively. The two consecutive reactions present an endothermic net heat, with total enthalpies in the order of 16–20 kcal mol^{-1} for *n*-dodecane and 13–19 kcal mol^{-1} for farnesane. The transition states and products formed in the farnesane molecule are more stabilized than in *n*-dodecane. The Supplementary material includes all tables and figures with the relative energies for each molecule calculated in this work.

In other to validate the construction of a mechanism incorporating only the H-abstraction and the β-scission to represent the initial steps of the fuel decomposition, we also studied other possible reaction paths. In special, we analyzed the bond dissociation paths, *i.e.*, those not requiring an external agent (in this case the hydrogen atom), calculating the change in Gibbs free energy ($\Delta_r G$) for all C–C and C–H bond dissociations as functions of the temperature. At 0 K, the lowest C–C and C–H bond dissociation enthalpies ($\Delta V_a^{G,\ddagger}$) are equal to 85.7 and 95.6 kcal mol^{-1} (*n*-dodecane), and 83.4 and 93.9 kcal mol^{-1} (farnesane), much higher that the activation enthalpy involved in H-abstraction and β-scission reactions. The difference of around 2 kcal mol^{-1} between the molecules consists of the difference between tertiary and secondary BDE.

The free energies of activation for a broad range of temperatures are collected in Fig. 3a, considering the lowest barrier heights calculated among all reactions studied for both *n*-dodecane and farnesane molecules. The H-abstraction presents the lowest activation free energy up to 800 K, and, from 800 to 1000 K, H-abstraction and β-scission present competitive free activation energies. Around 1200 K, the C–C break and β-scission present competitive free activation energy and above 1400 K, the C–C break is the reaction path with the lowest free activation energy. These results indicate that a mechanism including only H-abstraction and the β-scission should be favored in temperatures lower than 1200 K. This allowed using such a mechanism to describe the first steps in the fuel decomposition since the typical intermediaries formation for these fuel flames is in the temperature around 1000 K [5,29,6].

Fig. 3b shows the reaction rate constants (the highest and lowest values) for each type of reaction pathway which could be incorporated in the first step of the reaction mechanism (H-abstraction, and C–H and C–C breaks). For farnesane, the ratio between the lowest H-abstraction with the highest C–C break rate constants is still in the order of hundreds ($k_{\text{H-abstraction}}/k_{\text{C-C break}} \cong 400$) at 1200 K, which makes the C–C break competitive at this temperature in fuel-rich reaction systems. On the other hand, at 800 K, the $k_{\text{H-abstraction}}/k_{\text{C-C break}}$ is in the order of 10^9. It is worth noting that the reaction rates only become equal around 1500 K. As expected, the results for *n*-dodecane follows the same trend, but with a ratio between the rate constants tenfold higher at the same temperatures (10^{10} at 800 K, 4000 at 1200, and 10 at 1500 K). Therefore, we believe that the approximation of not including the C–C breaks is reasonable within the temperature range considered in this work and can be accurate in the lower temperatures (800–1000 K).

Tunneling corrections were introduced using the unidimensional Wigner approach in which is proportional to square the imaginary harmonic frequency ($\nu_i^{\ddagger}$) of the saddle point. As a result, higher values of the frequency result in higher values of tunneling corrections and consequently to the rate constants (Eq. (6)). In both molecules, the H-abstraction at the primary sites has the highest imaginary frequencies (from 1426*i* to 1456*i* cm^{-1}). Secondary and tertiary sites have structures, in which the saddle points frequencies are in the range of 1356*i* to 1389*i* cm^{-1}, except in the carbon 2 (*t*-site) of farnesane that results in 1421*i* cm^{-1}, due to this carbon been bounded to two primary carbons. Therefore, the transmission coefficients calculated with the $\nu_i^{\ddagger}$ multiplies the rate constants by 1.29 and 1.11 at 800 and 1200 K, respectively. The β-scission reactions present values of the $\nu_i^{\ddagger}$ from 532*i* to 640*i* cm^{-1}, and the reactions with methyl production have higher absolute values. These imaginary frequencies lead to factors of 1.22 and 1.04 in the rate constants at 800 and 1200 K, respectively.

3.2. Chemical kinetics of the H-abstraction reactions

The TST provides a good approximation of chemical kinetics from the electronic structure calculations at the high-pressure limit. Figs. 4a and 4b show the rate constants of forward H-abstraction and β-scission reactions of farnesane molecule, respectively. The complete data of thermal rate constants of the elementary reactions studied from 200 to

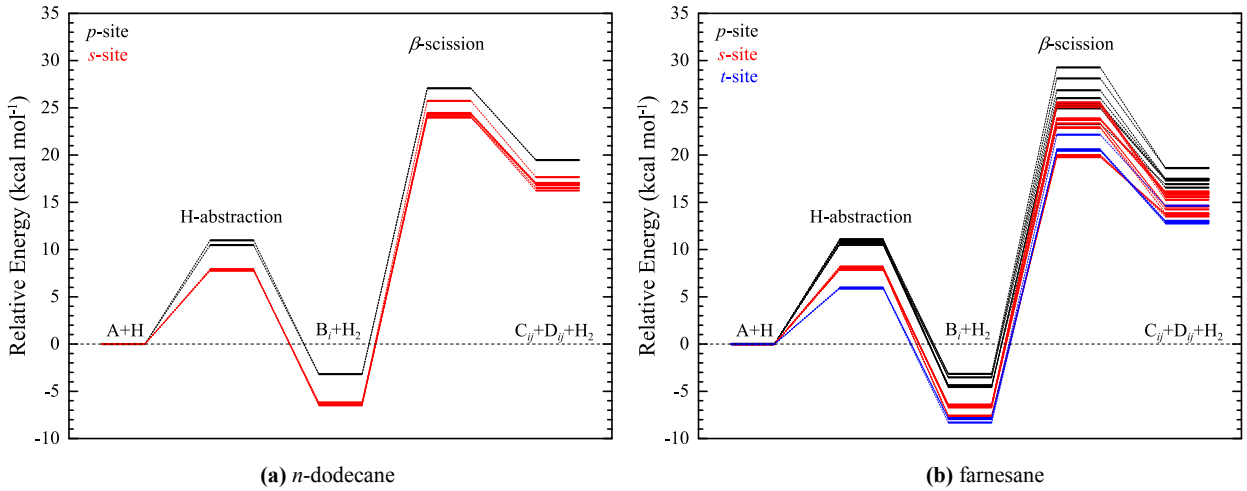


Fig. 2. Energy diagram associated to enthalpy of reactants for primary (*p*-site), secondary (*s*-site) and tertiary (*t*-site) of *n*-dodecane (2a) and farnesane (2)b, at 0 K.

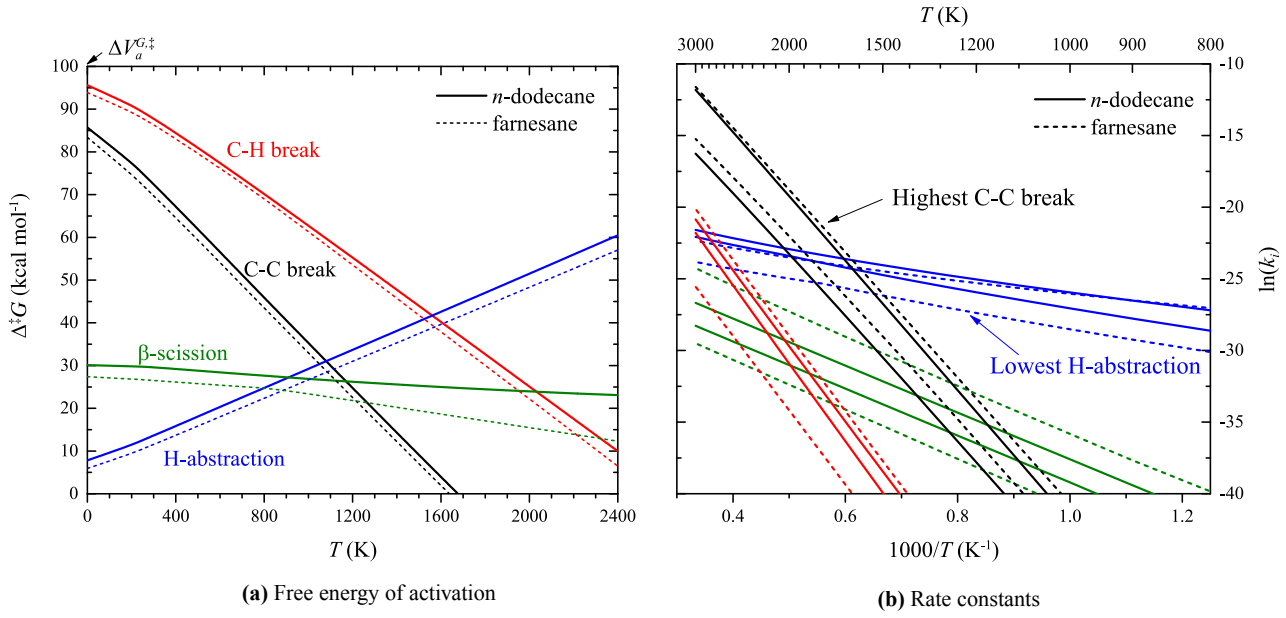


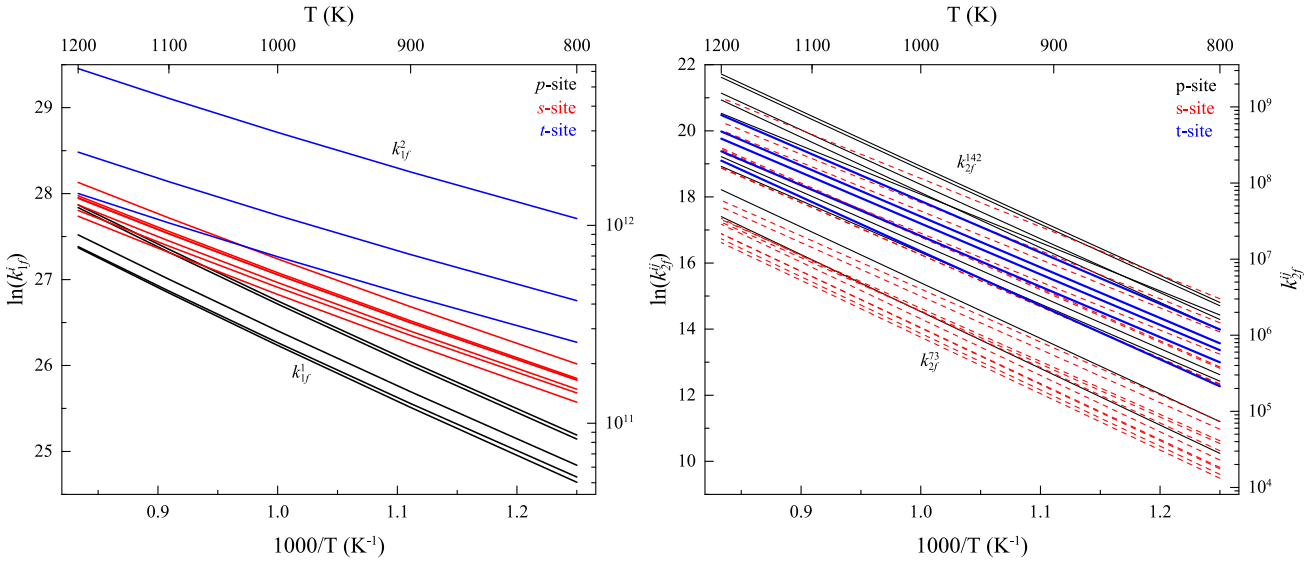
Fig. 3. (a) The free energy of activation for the lowest barrier heights of the H-abstraction and *β*-scissions reactions, and the lowest bond dissociation energies of the C–C and C–H breaks calculated for *n*-dodecane (solid lines) and farnesane (dash lines) molecules. (b) The highest and lowest rate constants for H-abstractions, *β*-scissions, and C–C and C–H breaks.

3000 K, as well as the figures containing the Arrhenius plots for all reactions studied in this work were collected in the Supplementary materials.

The slope of the natural logarithm of the Arrhenius equation is directly related to the activation energy (E_a) of the elementary reactions. Arrhenius plots presented here (from 800 K to 1200 K) show the trends for each site of the forward H-abstraction, as we see in Fig. 4a. There were three different activation energy ranges, where they differ by the *A*-factor. The highest reaction rates were observed in *t*-sites (k_{1f}^2 is the highest among then), follow by *s*-sites and *p*-sites (k_{1f}^1 was the lowest) up to 1000 K, respectively. Some *p*-site present higher rate constants than *s*-site reactions, as expected at higher temperatures. This tendency was observed in the values collected from Arrhenius parameters in Table 1. Although the activation energy was lower on *t*-sites than on *s*-sites, the change in behavior observed in rate constants above 1000 K, for secondary k_{1f}^4 and tertiary k_{1f}^6 of farnesane, was attributed to the *A*-factor of secondary sites being twice higher than tertiary. This behavior also occurred on *p*-sites k_{1f}^{12} and k_{1f}^{12} compared to the *s*-site k_{1f}^{11}.

The *A*-factors calculated herein for both fuel molecules were in order of 10^6 cm^3 mol^{-1} s^{-1}, the same order of magnitude presented by previous works on heptane [35], iso-octane [36] and methyl-cyclohexane [37]. The *b* parameters varied from 2.20 to 2.25 on farnesane and from 2.25 to 2.29 on *n*-dodecane molecules, close to the most common empirical values used in combustion mechanisms (2.40–2.54) from Orme's work [37]. The average calculated activation energy values for *p*-, *s*- and *t*-sites are overestimated by 1.7, 1.4 and 1.3 kcal mol^{-1}, respectively, in comparison to the results obtained by Orme *et al.* [37].

The reverse elementary reactions of farnesane (Fig. S23 of SM1) present a slower kinetics than the forward reactions (Fig. 4a), as expected from the energy profile showed in Fig. 2b for the first step (exothermal). Their rate constants were calculated to be approximately 10^3 times lower than the forward reactions, with E_a values around 10 kcal mol^{-1} (Table 1). The *p*-sites present the highest rates for the reverse reactions, in which k_{1r}^{14} and k_{1r}^{15} presents the highest values. These reactions involve a transition state on methyl radicals bonded with carbons 6 and 10. The calculated *A*-factors are in order of 10^1 cm^3 mol^{-1} s^{-1}, which were up to 10^2 times lower than other reverse



(a) Forward H-abstraction **(b)** Forward β-scission

Fig. 4. Arrhenius plots for all non-equivalent forward reaction pathways in the first step (a), H-abstraction (right axis in cm^3 mol^{-1} s^{-1}), and the second step (b), β-scission (right axis in s^{-1}), obtained with TST and Wigner corrections for the farnesane molecule.

reactions. However, the calculated b parameter of k^{14}_{1r} and k^{15}_{1r} of approximately 3.7 differs from other reverse reactions, which present b values around 2.7, meaning a collision frequency factor more sensitive to the temperature. In general, the frequency factor considering $A \times T^b$ presents higher values on primary sites, due to 3 possibilities of an attack on hydrogen-bonded to carbons follow by secondary and tertiary

Table 1
Arrhenius fitted parameters of the H-abstractions reactions from TST and M06-2X/maug-cc-pV(T + d)Z levels.

Elementary Reactions	Forward Parameters				Reverse Parameters			
	k^i_{1f}	A (cm^3 mol^{-1} s^{-1})	b	E_a (kcal mol^{-1})	k^i_{1r}	A (cm^3 mol^{-1} s^{-1})	b	E_a (kcal mol^{-1})
farnesane reactions								
$C_{15}H_{32}$ + ·H ⇌ p-$C_{15}H_{31}$–1 + H_2	k^1	3.87×10^6	2.23	8.68	k^1	2.94×10^3	2.69	9.55
$C_{15}H_{32}$ + ·H ⇌ t-$C_{15}H_{31}$–2 + H_2	k^2	4.16×10^6	2.24	3.99	k^2	6.53×10^2	2.83	10.0
$C_{15}H_{32}$ + ·H ⇌ s-$C_{15}H_{31}$–3 + H_2	k^3	2.42×10^6	2.21	5.95	k^3	1.37×10^2	2.72	9.97
$C_{15}H_{32}$ + ·H ⇌ s-$C_{15}H_{31}$–4 + H_2	k^4	2.65×10^6	2.22	5.77	k^4	1.04×10^3	2.68	11.1
$C_{15}H_{32}$ + ·H ⇌ s-$C_{15}H_{31}$–5 + H_2	k^5	2.16×10^6	2.21	5.85	k^5	3.26×10^2	2.72	10.0
$C_{15}H_{32}$ + ·H ⇌ t-$C_{15}H_{31}$–6 + H_2	k^6	1.22×10^6	2.21	3.98	k^6	1.11×10^2	2.81	9.74
$C_{15}H_{32}$ + ·H ⇌ s-$C_{15}H_{31}$–7 + H_2	k^7	2.43×10^6	2.21	5.84	k^7	3.69×10^2	2.71	10.1
$C_{15}H_{32}$ + ·H ⇌ s-$C_{15}H_{31}$–8 + H_2	k^8	2.37×10^6	2.21	5.78	k^8	1.11×10^3	2.68	11.2
$C_{15}H_{32}$ + ·H ⇌ s-$C_{15}H_{31}$–9 + H_2	k^9	2.70×10^6	2.20	5.87	k^9	5.60×10^2	2.71	10.1
$C_{15}H_{32}$ + ·H ⇌ t-$C_{15}H_{31}$–10 + H_2	k^{10}	1.76×10^6	2.22	3.94	k^{10}	2.30×10^2	2.82	9.63
$C_{15}H_{32}$ + ·H ⇌ s-$C_{15}H_{31}$–11 + H_2	k^{11}	2.13×10^6	2.21	6.04	k^{11}	4.77×10^2	2.71	10.4
$C_{15}H_{32}$ + ·H ⇌ p-$C_{15}H_{31}$–12 + H_2	k^{12}	5.03×10^6	2.25	8.41	k^{12}	4.53×10^3	2.68	10.5
$C_{15}H_{32}$ + ·H ⇌ p-$C_{15}H_{31}$–13 + H_2	k^{13}	5.28×10^6	2.25	8.50	k^{13}	2.52×10^3	2.71	9.67
$C_{15}H_{32}$ + ·H ⇌ p-$C_{15}H_{31}$–14 + H_2	k^{14}	3.75×10^6	2.23	8.47	k^{14}	1.71×10^1	3.68	10.5
$C_{15}H_{32}$ + ·H ⇌ p-$C_{15}H_{31}$–15 + H_2	k^{15}	3.80×10^6	2.24	8.44	k^{15}	1.64×10^1	3.69	10.5
n-dodecane reactions								
$C_{12}H_{26}$ + ·H ⇌ p-$C_{12}H_{25}$–1 + H_2	k^1	9.64×10^6	2.29	8.36	k^1	8.40×10^2	2.74	9.30
$C_{12}H_{26}$ + ·H ⇌ s-$C_{12}H_{25}$–2 + H_2	k^2	8.92×10^6	2.28	5.85	k^2	7.31×10^2	2.75	10.1
$C_{12}H_{26}$ + ·H ⇌ s-$C_{12}H_{25}$–3 + H_2	k^3	7.17×10^6	2.26	5.72	k^3	6.13×10^2	2.75	9.76
$C_{12}H_{26}$ + ·H ⇌ s-$C_{12}H_{25}$–4 + H_2	k^4	6.71×10^6	2.27	5.67	k^4	5.61×10^2	2.76	9.77
$C_{12}H_{26}$ + ·H ⇌ s-$C_{12}H_{25}$–5 + H_2	k^5	7.03×10^6	2.25	5.73	k^5	3.64×10^2	2.71	9.91
$C_{12}H_{26}$ + ·H ⇌ s-$C_{12}H_{25}$–6 + H_2	k^6	6.19×10^6	2.26	5.70	k^6	2.65×10^2	2.72	9.89
Parameters from literature								
n-propane + ·H ⇌ p-propyl + H_2	a	1.32×10^6	2.54	6.756	a	1.81×10^3	2.84	9.141
	b	3.49×10^5	2.69	6.450				
i-butane + ·H ⇌ p-butyl + H_2	a	1.81×10^6	2.54	6.756	a	2.83×10^3	2.72	9.797
	c	1.88×10^5	2.75	6.280				
n-propane + ·H ⇌ s-propyl + H_2	a,b	1.30×10^6	2.40	4.471	a	3.49×10^2	3.28	8.670
	c	5.74×10^5	2.49	4.124				
i-butane + ·H ⇌ t-butyl + H_2	a,b,c	6.02×10^5	2.40	2.583	a	1.85×10^{-2}	4.24	8.962

[a] Chemical kinetic data base for n-propane [33] and i-butane [34]. [b] Zhang's work for n-heptane oxidation [38]. [c] Curran's work for iso-octane oxidation [36].

Table 2
Arrhenius fitted parameters of the β-scission reactions from TST and M06-2X/maug-cc-pV(T + d)Z levels.

Elementary Reactions	Forward Parameters				Reverse Parameters			
	k_{2f}^{ij}	A (s^{-1})	b	E_a (kcal mol^{-1})	k_{2r}^{ij}	A (cm^3 mol^{-1} s^{-1})	b	E_a (kcal mol^{-1})
farnesane reactions								
p-$C_{15}H_{31}$–1 ⇌ C_3H_6 + ·$C_{12}H_{25}$	k^{11}	9.78×10^{12}	0.317	30.8	k^{11}	1.18×10^{-2}	4.03	7.46
p-$C_{15}H_{31}$–1 ⇌ $C_{14}H_{28}$ + ·CH_3	k^{12}	2.45×10^{12}	0.406	33.4	k^{12}	2.85×10^{0}	3.00	8.22
t-$C_{15}H_{31}$–2 ⇌ C_4H_8 + ·$C_{11}H_{23}$	k^{21}	7.76×10^{12}	0.478	30.0	k^{21}	2.45×10^{1}	2.99	6.44
s-$C_{15}H_{31}$–3 ⇌ $C_{14}H_{28}$-2 + ·CH_3	k^{31}	9.10×10^{11}	0.441	32.8	k^{31}	1.15×10^{1}	2.99	7.01
s-$C_{15}H_{31}$–3 ⇌ C_5H_{10} + ·$C_{10}H_{21}$	k^{32}	9.18×10^{11}	0.389	31.1	k^{32}	6.77×10^{0}	2.98	6.38
s-$C_{15}H_{31}$–3 ⇌ $C_{14}H_{28}$-2 + ·CH_3	k^{33}	1.13×10^{12}	0.463	32.6	k^{33}	1.40×10^{1}	3.00	6.96
s-$C_{15}H_{31}$–4 ⇌ $C_{12}H^{24}$ + ·C_3H_7-2	k^{41}	8.47×10^{12}	0.313	28.5	k^{41}	1.57×10^{0}	3.05	4.78
s-$C_{15}H_{31}$–4 ⇌ C_6H_{12} + ·C_9H^{19}-2	k^{42}	2.24×10^{13}	0.305	28.4	k^{42}	4.63×10^{0}	3.06	4.68
s-$C_{15}H_{31}$–5 ⇌ $C_{11}H^{22}$ + ·C_4H_9	k^{51}	1.47×10^{12}	0.395	31.3	k^{51}	4.05×10^{0}	2.98	6.20
s-$C_{15}H_{31}$–5 ⇌ C_8H^{16} + ·C_7H_{15}	k^{52}	8.17×10^{12}	0.374	30.8	k^{52}	3.70×10^{-2}	4.04	7.16
s-$C_{15}H_{31}$–5 ⇌ $C_{14}H_{28}$-5 + ·CH_3	k^{53}	7.48×10^{11}	0.460	33.1	k^{53}	6.12×10^{0}	3.00	7.65
t-$C_{15}H_{31}$–6 ⇌ $C_{10}H_{20}$ + ·C_5H_{11}	k^{61}	3.17×10^{12}	0.478	29.6	k^{61}	8.55×10^{0}	3.00	6.13
t-$C_{15}H_{31}$–6 ⇌ C_9H_{18} + ·C_6H_{13}	k^{62}	2.05×10^{12}	0.482	29.5	k^{62}	7.26×10^{0}	3.00	6.20
s-$C_{15}H_{31}$–7 ⇌ C_9H_{18}-2 + ·C_6H_{13}	k^{71}	9.82×10^{12}	0.356	30.9	k^{71}	4.12×10^{0}	3.04	7.14
s-$C_{15}H_{31}$–7 ⇌ $C_{10}H^{22}$ + ·C_5H_{11}	k^{72}	1.03×10^{12}	0.384	31.1	k^{72}	4.11×10^{0}	2.98	6.36
s-$C_{15}H_{31}$–7 ⇌ $C_{14}H_{28}$-6 + ·CH_3	k^{73}	8.46×10^{11}	0.432	33.1	k^{73}	5.84×10^{0}	3.00	7.66
s-$C_{15}H_{31}$–8 ⇌ C_7H_{14} + ·C_8H^{17}-2	k^{81}	9.68×10^{12}	0.319	28.3	k^{81}	1.97×10^{0}	3.06	4.70
s-$C_{15}H_{31}$–8 ⇌ $C_{11}H^{22}$ + ·C_4H_9-2	k^{82}	4.63×10^{12}	0.303	28.5	k^{82}	9.72×10^{-1}	3.04	4.70
s-$C_{15}H_{31}$–9 ⇌ C_6H_{12} + ·C_9H^{19}	k^{91}	1.78×10^{12}	0.387	31.1	k^{91}	4.88×10^{0}	2.98	6.34
s-$C_{15}H_{31}$–9 ⇌ $C_{13}H_{26}$-2 + ·C^2H_5	k^{92}	3.37×10^{12}	0.389	30.4	k^{92}	3.00×10^{0}	3.02	7.20
s-$C_{15}H_{31}$–9 ⇌ $C_{14}H_{28}$-3 + ·CH_3	k^{93}	1.47×10^{12}	0.433	33.2	k^{93}	6.28×10^{0}	2.97	7.66
t-$C_{15}H_{31}$–10 ⇌ C_5H_{10} + ·$C_{10}H_{21}$	k^{101}	4.04×10^{12}	0.478	29.6	k^{101}	1.89×10^{1}	2.99	6.30
t-$C_{15}H_{31}$–10 ⇌ $C_{14}H_{28}$ + ·CH_3	k^{102}	1.84×10^{12}	0.570	31.4	k^{102}	2.62×10^{1}	2.98	5.42
s-$C_{15}H_{31}$–11 ⇌ C_4H_8-2 + ·$C_{11}H_{23}$	k^{111}	4.35×10^{12}	0.369	30.6	k^{111}	1.94×10^{-2}	4.05	6.92
s-$C_{15}H_{31}$–11 ⇌ $C_{14}H_{28}$-2 + ·CH_3	k^{112}	9.48×10^{11}	0.447	33.0	k^{112}	4.42×10^{0}	2.99	7.68
p-$C_{15}H_{31}$–12 ⇌ C^2H_4 + ·$C_{13}H_{27}$-2	k^{121}	2.15×10^{13}	0.256	28.6	k^{121}	2.10×10^{0}	3.05	4.58
p-$C_{15}H_{31}$–13 ⇌ $C_{14}H_{28}$ + ·CH_3	k^{131}	3.98×10^{12}	0.409	32.6	k^{131}	6.82×10^{0}	3.00	7.19
p-$C_{15}H_{31}$–13 ⇌ C_3H_6 + ·$C_{12}H_{25}$	k^{132}	5.50×10^{12}	0.327	30.3	k^{132}	9.22×10^{-3}	4.04	6.62
p-$C_{15}H_{31}$–14 ⇌ C_9H_{18} + ·C_6H_{13}	k^{141}	6.20×10^{10}	1.34	30.3	k^{141}	1.14×10^{0}	3.05	6.25
p-$C_{15}H_{31}$–14 ⇌ C_8H^{16} + ·C_7H_{15}	k^{142}	7.57×10^{10}	1.33	30.4	k^{142}	1.47×10^{-2}	4.05	6.28
p-$C_{15}H_{31}$–15 ⇌ C_4H_8 + ·$C_{11}H_{23}$	k^{151}	3.96×10^{10}	1.32	30.6	k^{151}	1.16×10^{-2}	4.05	6.27
p-$C_{15}H_{31}$–15 ⇌ $C_{13}H_{26}$ + ·C^2H_5	k^{152}	3.73×10^{10}	1.33	30.1	k^{152}	1.53×10^{0}	3.02	6.47
n-dodecane reactions								
p-$C_{12}H_{25}$–1 ⇌ C^2H_4 + ·$C_{10}H_{21}$	k^{11}	3.98×10^{12}	0.369	31.0	k^{11}	3.96×10^{0}	3.01	5.73
s-$C_{12}H_{25}$–2 ⇌ C_3H_6 + ·C_9H^{19}	k^{21}	4.52×10^{12}	0.398	31.5	k^{21}	2.62×10^{0}	3.02	5.90
s-$C_{12}H_{25}$–3 ⇌ $C_{11}H^{22}$ + ·CH_3	k^{31}	3.22×10^{12}	0.499	33.1	k^{31}	2.92×10^{1}	2.98	5.94
s-$C_{12}H_{25}$–3 ⇌ C_4H_8 + ·C_8H^{17}	k^{32}	5.40×10^{12}	0.403	31.0	k^{32}	2.79×10^{0}	3.02	5.29
s-$C_{12}H_{25}$–4 ⇌ $C_{10}H_{20}$ + ·C^2H_5	k^{41}	5.62×10^{12}	0.406	31.3	k^{41}	7.79×10^{0}	2.99	6.05
s-$C_{12}H_{25}$–4 ⇌ C_5H_{10} + ·C_7H_{15}	k^{42}	1.36×10^{13}	0.405	31.5	k^{42}	7.81×10^{0}	3.02	5.83
s-$C_{12}H_{25}$–5 ⇌ C_9H_{18} + ·C_3H_7	k^{51}	5.89×10^{12}	0.377	31.7	k^{51}	3.87×10^{0}	3.02	5.78
s-$C_{12}H_{25}$–5 ⇌ C_6H_{12} + ·C_6H_{13}	k^{52}	3.54×10^{12}	0.374	31.6	k^{52}	3.91×10^{0}	3.00	5.91
s-$C_{12}H_{25}$–6 ⇌ C_8H^{16} + ·C_4H_9	k^{61}	5.00×10^{12}	0.389	31.6	k^{61}	8.09×10^{-2}	4.01	5.87
s-$C_{12}H_{25}$–6 ⇌ C_7H_{14} + ·C_5H_{11}	k^{62}	3.72×10^{12}	0.373	31.6	k^{62}	3.62×10^{0}	3.00	5.88
Parameters from literature								
alkyl ⇌ terminal alkene + alkyl	a					8.5×10^{10}		7.800
alkyl ⇌ internal alkene + alkyl	a					8.5×10^{10}		10.600
p-octyl ⇌ ethene + 1-hexyl	b	9.12×10^{11}	0.31	27.238				
p-alkyl ⇌ alkene + alkyl	c	1.60×10^{13}	0.13	28.879				
s/t-alkyl ⇌ alkene + alkyl	c	1.38×10^{13}	0.17	29.912				
s-octyl ⇌ alkene + alkyl	d	6.0×10^{11}	0.50	27.650				
s-octyl ⇌ 1-heptene + methyl	b	9.55×10^{9}	1.08	29.388				
s-5MeH ⇌ alkene + methyl	e	2.79×10^{13}	0.16	28.450				
s-5MeH ⇌ alkene-2 + methyl	e	6.20×10^{13}	0.11	30.525				
s-5MeH ⇌ alkene + ethyl	e	4.48×10^{13}	0.033	28.976				
s-5MeH ⇌ propene + alkyl	e	2.36×10^{13}	0.07	27.109				

[a] Curran's works for *n*-heptane [35] and iso-octane [36]. [b] Tsang's work for octyl radicals [40]. [c] Ratkiewicz's work for alkyl radicals [42]. [d] Sarathy's work for 2-methylalkanes from C_7 to C_{20} radicals. [44]. Best fit to data in Ref. [40]. [e] Awan's work for 5-Methylhex-1-yl (5MeH) radical [41]. *A*-factor was multiplied herein by 297^b.

sites in the forward reactions. The only exception was the k_{1f}^2 tertiary site reaction of farnesane, which is among the highest pre-exponential factors (third-highest), close to *p*-sites values.

3.3. Chemical kinetics of the ß-scission elementary reactions

The Arrhenius fitted parameters of β-scission reactions are collected in Table 2, while the Arrhenius plots are shown in the Supplementary

material. The forward reactions consist in unimolecular reactions from $\cdot C_1–C_2–C_3$ radical break to form $C_1 = C_2$ and $\cdot C_3$ radical. These reactions present high activation energies, in the range of 28.3 to 33.4 kcal mol^{-1} for farnesane molecule and 31.0 to 33.1 kcal mol^{-1} for *n*-dodecane molecule. Reactions involving the production of methyl radicals have the highest values (~33 kcal mol^{-1}) for both molecules. On the other hand, the reactions with the lowest activation energies are those with the radical formed in secondary carbons, lying around 28.5 kcal mol^{-1} for farnesane. The remaining reactions forming heavier primary radicals present E_a values around 30 and 31 kcal mol^{-1} for farnesane and *n*-dodecane, respectively. The pre-exponential factors calculated as AT^b at 800 K have values in the range of 10^{13} s^{-1} to 5×10^{14} s^{-1} for the reactions k_{2f}^{32} and k_{2f}^{142}, respectively, within the same order of the literature range values (from 5×10^{12} s^{-1} [40] to 10^{14} s^{-1} [41]).

Thermal rate constants obtained for farnesane β-scission reactions presented larger variations, from 10^4 to 10^6 s^{-1} at 800 K, while *n*-dodecane presented values in the order of 10^5 s^{-1} at same temperature. The lower reaction rates on farnesane involve the formation of a methyl radical (from C_{13}, C_{14} and C_{15} bond dissociation with their respective tertiary carbons) and the formation of internal alkenes (double bonds does not involve terminal carbons). On the other hand, the faster reactions involve the formation of terminal alkenes and two kinds of alkyl radicals, secondary alkyl from H-abstraction in *s*-site (C_4) and mainly primary alkyl radicals from *p*-sites (C_{14} and C_{15}).

The reverse β-scission reaction from Table 2 present a frequency factor AT^b in the order of 10^9 and 10^{10} cm^3 mol^{-1} s^{-1} at 800 K and 1200 K, respectively, similar to recommendations of Curran's reference therein [35,36]. The E_a of farnesane terminal alkenes reactions have shown slight differences compared to Curran's works [35,36]. The lowest β-scission reaction activation energies are around 4.6 kcal mol^{-1} and are relative to reactions of terminal alkenes with secondaries alkyl radicals.

3.4. Thermal decomposition mechanism

Each elementary reaction obtained in Sections 3.2 and 3.3 for H-abstraction and β-scission, respectively, can be combined into an additive mechanism, *i.e.* each of those reactions is independent of each other and can be used as a model to calculate the molar fractions of all species. All concentration values were obtained by the mechanism from 800 to 1200 K and 10^{-10} s to 10 s (available in the Supplementary material). The molar fractions obtained at 800 K from 10^{-9} to 10 s for the *n*-dodecane and farnesane mechanisms were shown in Fig. 5a. The results for 10^{-2} s (800 to 1200 K) are presented in Fig. 5b, which includes the molar fraction of ethene (C_2H_4), propene (C_3H_6), but-1-ene (C_4H_8), methyl (CH_3), ethyl (C_2H_5) and the intermediate species produced by them.

The concentrations of the fuels (*n*-dodecane or farnesane) and hydrogen radical starts with molar fractions equal to 0.5 for each species. The initial molar fraction of fuels *n*-dodecane or farnasane, and hydrogen radical was set to 0.5. The *n*-dodecane was consumed slightly faster than farnesane. They approach equilibrium with intermediate species after 10^{-5} s, remaining less than 1% of the reactants. Intermediate species achieve the maximum molar fractions between 10^{-6} s and 10^{-3} s, when the β-scission products begin to be formed. These results are in agreement with Mzé-Ahmed *et al.* [61] that have simulated the total fuel consumption of *n*-dodecane as less than 10^{-4} s and the ignition delay times at 10^{-3} s to farnesane [27,30] and to *n*-dodecane [62,63].

The molar fractions (x_i) of the species included in the *n*-dodecane reactions were larger than those species included in the farnesane reactions. The higher molar fraction in the *n*-dodecane reactions was obtained due to the lower number of molecules included in the mechanism, where the total concentration represents the sum of 20 molecules, while for farnesane is the sum of the 49 molecules. The pathway for the formation of β-scission products shows in Fig. 5a for *n*-dodecane depends exclusively on one type of intermediate alkyl (for each product), obtained by the radicals $C_{12}H_{25}$-1, 2, 3 and 4. However, using farnesane as initial fuel, only the ethene and but-1-ene products are connected through a single reaction path, via $C_{15}H_{31}$-12 and 15, respectively. In farnesane mechanism, propene is formed from two pathways (via $C_{15}H_{31}$-1 and 13 radicals), while the methyl radical can be obtained from nine pathways and eight different intermediaries species, as follow, $C_{15}H_{31}$-1, 3, 5, 7, 9, 10, 11 and 13. Also, the ethyl radical can be obtained from two pathways (via $C_{15}H_{31}$-9 and 15).

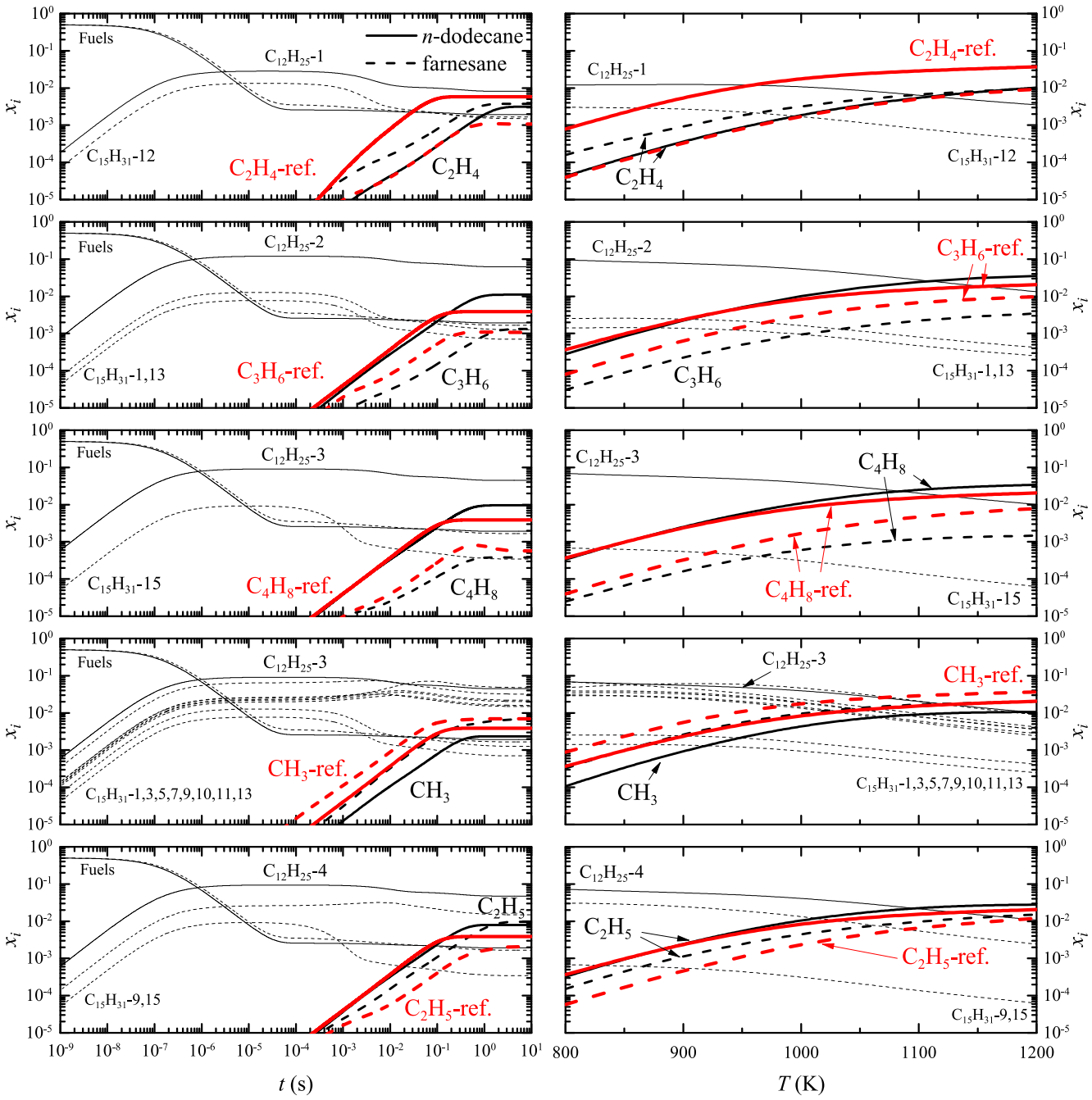
The temperature dependence (after 10^{-2} s) can be seen in Fig. 5b, in which the molar fractions of the intermediates decrease when increasing the temperature, while the products increase by 2 orders of magnitude from 800 to 1200 K. The molar fraction of the β-scission products of *n*-dodecane exceeds intermediate species at temperatures above 1080 K, while for farnesane this occurs at lower temperatures, above 870 K.

Propene (C_3H_6) is an important soot precursor molecule since it forms the propargyl radical (C_3H_3), from which benzene and phenyl formation pathways can be obtained by the propargyl self-reaction [1,11,43]. The calculated molar fraction of propene is 3×10^{-4} at 800 K and 10^{-2} s in the *n*-dodecane mechanism, a value 9 times higher than the molar fraction obtained in farnesane mechanism in the same conditions. In all of the analyzed temperature range, the formation of propene is higher for *n*-dodecane than for farnesane. The C_3H_6 molecule is obtained from the β-scission of the $C_{12}H_{25}$-2 radical formed by the hydrogen abstracted from the secondary C_2 site of *n*-dodecane, in which it has the highest rate constant among all H-abstraction reactions of the *n*-dodecane. On the other hand, for farnesane, the C_3H_6 molecule is formed from the primary carbons ($C_{15}H_{31}$-1 and 13), thus becomes slower in comparison to the available sites in the farnesane molecule.

But-1-ene (C_4H_8) is another product in the present mechanism that can lead to soot precursors (benzene) through the $C_4H_8 \rightarrow C_4H_7 \rightarrow C_4H_6 \rightarrow C_4H_5$ route, followed by its reaction with ethene to form benzene [6]. The ethene and but-1-ene molar fractions are directly connected to the type of radical that form them. C_2H_4 were formed from *p*-alkyl radicals, and the larger amount in farnesane was due to the β-scission secondary counter products ($C_{13}H_{27}$-2) presenting lower activation energy than primary product ($C_{10}H_{21}$) in *n*-dodecane. On other hand, C_4H_8 was formed through *s*-alkyl in *n*-dodecane and *p*-alkyl in farnesane. Therefore, H-abstraction was the limiting factor for its formation and the molar fraction on farnesane mechanism was in the order of 10^{-5}, while it was one order of magnitude higher in *n*-dodecane at lower temperatures (see Fig. 5b).

The formation of methyl radicals (CH_3) is higher for the farnesane molecule, with the molar fraction in order of 3×10^{-4} at 10^{-2} s and 800 K, 3 times higher than in *n*-dodecane molecule. Experimental results based on the peak molar fractions have shown that the elimination of a methyl group is favored in farnesane decomposition [29]. The CH_3 produced is mainly due to the presence of the three branches in the carbon chain of the farnesane molecule. Thus, the CH_3 can be produced from 9 different β-scission reactions, whereas in the *n*-dodecane molecule the radical CH_3 is formed only by the one β-scission.

In general, the maximum molar fractions of formed products were found below 1 s in farnesane from reactions k_2^{41}, k_2^{42}, k_2^{81}, k_2^{61}, k_2^{82}, k_2^{62} and k_2^{21}, in which the fourth and sixth reactions are in agreement with those of Oßwald [29], who detected $C_{10}H_{20}$ and C_9H_{18} products with significant molar fraction in their experiments involving the combustion of farnesane at 900 K. Some generated species were similar to the ones produced at the Richter's mechanism [30], where the H-abstraction reaction paths are responsible to produce *s*-$C_{15}H_{31}$. In *n*-dodecane mechanism the maximum molar fraction of products was obtained around 1 s for k_2^{62}, k_2^{21}, k_2^{51} and k_2^{42} at 800 K, in which the first reaction that produces C_7H_{14} and C_5H_{11} is in agreement with the measurements in flow reactor [6]. Also, the smallest molar fraction obtained was in reaction k_2^{31}, which is responsible to produce the methyl radical. The intermediate species concentration of *n*-dodecane follows the order at



(a) Molar fraction at 800 K **(b)** Molar fraction at 10^{-2} s

Fig. 5. Molar fractions (from top to bottom) of ethene, propene, but-1-ene, methyl and ethyl molecules obtained within the reaction sub-mechanism for *n*-dodecane (solid) and farnesane (dashed). The left side (5a) shows the results as a function of time (at 800 K), while the right side (5b) shows the results as a function of the temperature (after 10^{-2} s). The curves in red present the results obtained by using the kinetic parameters available in the literature [33,34,38,36,42] within the same sub-mechanism.

1000 K: $C_{12}H_{25}$-6 (32%) > $C_{12}H_{25}$-5 (26%) > $C_{12}H_{25}$-2 (16%) > $C_{12}H_{25}$-4 (12%) ≈ $C_{12}H_{25}$-3 (12%) ≫ $C_{12}H_{25}$-1 (3%), indicating that our reduced sub-mechanism is similar to the optimized model available in the literature parameterized from experimental data [5].

When solving the sub-mechanism proposed in this work using the kinetic parameters from the literature (red curves in Fig. 5a and b instead of the calculated values one can see some important differences. The following discussion considers this condition. In the case of ethene, there is an inversion in which fuel generates the highest molar fraction of this substance. For the other species there is a qualitative (or ordering) agreement but with some important quantitative differences as shown in Table 3.

The formation of the but-1-ene presents the best agreement between the results obtained with the use of calculated kinetic parameters or the parameters from the literature, especially in the time range from 10^{-3} to 10^{-1} s. Overall, there is a better agreement between the calculated and literature data for *n*-dodecane than for farnesane, as expected, since the kinetic parameters used in the literature do not grasp some effects of the fuel structure, and this effect is expected to be more important in the branched species.

We believe that the most important change resides precisely in the

Table 3
Molar fraction of the selected molecules produced in the sub-mechanism representing the first fuel decomposition steps for *n*-dodecane and farnesane, after 10^{-2} s and at 800 K. The results were obtained by using kinetic parameters from quantum chemistry (calculated) and also from estimatives used in mechanism available in the literature [33,34,38,36,42].

	n-dodecane			farnesane		
Molecules	calculated	literature	calculated/literature	calculated	literature	calculated/literature
C_2H_4	4.26×10^{-5}	7.92×10^{-4}	0.1	1.59×10^{-4}	3.97×10^{-5}	4.0
C_3H_6	2.79×10^{-4}	3.71×10^{-4}	0.8	3.08×10^{-5}	7.94×10^{-5}	0.4
C_4H_8	3.34×10^{-4}	3.70×10^{-4}	0.9	2.49×10^{-5}	3.97×10^{-5}	0.6
CH_3	1.07×10^{-4}	3.70×10^{-4}	0.3	3.24×10^{-4}	8.89×10^{-4}	0.4
C_2H_5	3.22×10^{-4}	3.70×10^{-4}	0.9	1.51×10^{-4}	5.80×10^{-5}	2.6

description of the β-scission on a tertiary carbon. The mechanisms from the literature uses the same kinetic parameters for the β-scission on all secondary and tertiary carbons, with $A = 1.38 \times 10^{13}\ s^{-1}$; $b = 0.17$ and $E_a = 29.912\ kcal\ mol^{-1}$ [42]. On the other hand, the calculated values differ significantly for secondary ($A = 7.48 - 224 \times 10^{11}\ s^{-1}$; $b = 0.305 - 0.463$; $E_a = 28.3 - 33.2\ kcal\ mol^{-1}$) and tertiary ($A = 1.84 - 7.76 \times 10^{12}\ s^{-1}$; $b = 0.478 - 0.570$; $E_a = 29.5 - 31.4\ kcal\ mol^{-1}$) β-scissions and depend on the specific cleavage position, as can be seen in Fig. 4b.

4. Conclusions

This work has used methods of computational chemistry to study the formation of soot precursors involving the first steps of alkanes decomposition. Specifically, the farnesane and *n*-dodecane decompositions were analyzed using a sub-mechanism containing all elementary reactions involved in H-abstraction and β-scission reactions. The thermochemical and kinetic parameters were obtained by DFT calculations with the conventional TST methodology. The rate constants and kinetic parameters were calculated at intermediate temperatures (from 800 to 1200 K) for those elementary reactions and can be useful to update the parameters used in popular fuel decomposition mechanisms.

A key aspect in the molecular quantum chemistry approach is that the kinetic parameters of the elementary reactions are “parameter-free”, *i.e.*, they are not reconstructed from the experimental data and, therefore, are free from possible artificial effects that rises from incorporating the “infinite mechanism” of nature into the parameterized “finite” models. This parameterized models can describe with high accuracy molar fraction of reactants, intermediates, and products for the experiment in which they were parameterized, but may not represent the molecular processes and can have limited applications outside the conditions for which they were parametrized. Therefore these elementary reaction rate constants may fail when used in other reaction systems (or different conditions). On the other hand, mechanisms derived from thermochemical and kinetics calculations are additive and can be incorporated in other larger mechanisms, been limited essentially by the number of reaction paths described (including their conditions, *e.g.* solvents, catalysts).

In general, our results indicate the H-abstraction in C_4, C_6 and C_8 (for farnesane) and in C_4 and C_2 (for *n*-dodecane) positions as the favored first step in the decomposition of these fuels. The chosen methodology was able to identify the molar fractions in both fuel sub-mechanisms, revealing that farnesane yields a smaller amount of species responsible to release soot precursors, due to the position of the branched carbons that determines the most important sites in H-abstraction reactions, which in turn influences the subsequent rate of reaction that produces those soot precursors. Also, the calculated values of molar fractions are in reasonable agreement with the experimental and simulated data available in the literature.

The propene and but-1-ene concentrations obtained for *n*-dodecane were around 9 and 13 times higher, respectively than for farnesane, showing that the main reactants for the production of benzene precursors are present in lower concentrations in the farnesane decomposition. The molar fraction of ethene and methyl radical is about 3 times higher in the farnesane mechanism. Although they may also produce a benzene molecule, the route through methyl is less important compared to the $C_3 + C_3$ and $C_2 + C_4$ routes. Also, the ethene route depends on C_4 species that was produced in small quantities in farnesane decomposition.

Finally, it was showed that computational chemistry can be used to aid in the design of new fuels that are more efficient and/or less polluting, by investigating, for example, the first steps of a fuel decomposition in a reduced mechanism, avoiding the complexity of a complete mechanism, while also generating fairly accurate kinetic parameters for elementary reactions. These reactions can be used in other mechanisms representing experimental setups in different contexts.

CRediT authorship contribution statement

Marcelo André Petry Pontes: Investigation, Software, Formal analysis, Data curation, Writing - original draft. **Francisco Bolivar Correto Machado:** Methodology, Writing - review & editing, Resources, Funding acquisition. **Orlando Roberto-Neto:** Conceptualization, Methodology, Writing - review & editing, Funding acquisition, Project administration. **Luiz Fernando de Araujo Ferrão:** Conceptualization, Methodology, Formal analysis, Validation, Writing - review & editing, Funding acquisition, Supervision.

Declaration of Competing Interest

The authors declare that they have no known competing financial interests or personal relationships that could have appeared to influence the work reported in this paper.

Acknowledgments

This study was financed in part by the Coordenação de Aperfeiçoamento de Pessoal de Nível Superior – Brasil (CAPES) – Finance Code 001. This work was also supported by the COMAER PROPHIPER 14-X project. The authors also thank Brazilian agencies Fundação de Amparo à Pesquisa do Estado de São Paulo (FAPESP) under grants 2019/03729-8 and 2017/07707-3, Conselho Nacional de Desenvolvimento Científico e Tecnológico (CNPq) under grants 307052/2016-8, 404337/2016-3, 304789/2016-0, 309051/2016-9 and 406107/2016-5.

Appendix A. Supplementary data

Supplementary data associated with this article can be found, in the online version, at https://doi.org/10.1016/j.fuel.2020.117334.

References

[1] McEnally CS, Pfefferle LD, Atakan B, Kohse-Höinghaus K. Studies of aromatic hydrocarbon formation mechanisms in flames: Progress towards closing the fuel gap. Prog Energy Combust Sci 2006;32(3):247–94. https://doi.org/10.1016/j.pecs.2005.

11.003.
[2] Ruwe L, Moshammer K, Hansen N, Kohse-Höinghaus K. Consumption and hydrocarbon growth processes in a 2-methyl-2-butene flame. Combust Flame 2017;175:34–46. https://doi.org/10.1016/j.combustflame.2016.06.032.
[3] Ruwe L, Moshammer K, Hansen N, Kohse-Höinghaus K. Influences of the molecular fuel structure on combustion reactions towards soot precursors in selected alkane and alkene flames. Phys Chem Chem Phys 2018;20(16):10780–95. https://doi.org/10.1039/c7cp07743b.
[4] Tang Q, Wang M, You X. Measurements of sooting limits in laminar premixed burner-stabilized stagnation ethylene, propane, and ethylene/toluene flames. Fuel 2019;235:178–84. https://doi.org/10.1016/j.fuel.2018.07.090.
[5] Banerjee S, Tangko R, Sheen DA, Wang H, Bowman CT. An experimental and kinetic modeling study of n-dodecane pyrolysis and oxidation. Combust Flame 2016;163:12–30. https://doi.org/10.1016/j.combustflame.2015.08.005.
[6] Kathrotia T, Oßwald P, Köhler M, Slavinskaya N, Riedel U. Experimental and mechanistic investigation of benzene formation during atmospheric pressure flow reactor oxidation of n-hexane, n-nonane, and n-dodecane below 1200 K. Combust Flame 2018;194:426–38. https://doi.org/10.1016/j.combustflame.2018.05.027.
[7] Wang H, Li Y, Iqbal Z, Wang Y, Ma C, Yao M. A comparison study on the combustion and sooting characteristics of base engine oil and n-dodecane in laminar diffusion flames. Appl Therm Eng 2019;158:1–6. https://doi.org/10.1016/j.applthermaleng.2019.113812. 113812.
[8] Han S, Li X, Nie F, Zheng M, Liu X, Guo L. Revealing the initial chemistry of soot nanoparticle formation by ReaxFF molecular dynamics simulations. Energy Fuels 2017;31(8):8434–44. https://doi.org/10.1021/acs.energyfuels.7b01194.
[9] Han S, Li X, Zheng M, Guo L. Initial reactivity differences between a 3-component surrogate model and a 24-component model for RP-1 fuel pyrolysis evaluated by ReaxFF MD. Fuel 2018;222:753–65. https://doi.org/10.1016/j.fuel.2018.02.112.
[10] Ashraf C, Shabnam S, Jain A, Xuan Y, van Duin AC. Pyrolysis of binary fuel mixtures at supercritical conditions: a ReaxFF molecular dynamics study. Fuel 2019;235:194–207. https://doi.org/10.1016/j.fuel.2018.07.077.
[11] Hansen N, Cool TA, Westmoreland PR, Kohse-Höinghaus K. Recent contributions of flame-sampling molecular-beam mass spectrometry to a fundamental understanding of combustion chemistry. Prog Energy Combust Sci 2009;35(2):168–91. https://doi.org/10.1016/j.pecs.2008.10.001.
[12] Kohse-Höinghaus K, Oßwald P, Cool TA, Kasper T, Hansen N, Qi F, et al. Biofuel combustion chemistry: from ethanol to biodiesel. Angew Chem Int Ed Engl 2010;49(21):3572–97. https://doi.org/10.1002/anie.200905335.
[13] Peralta-Yahya PP, Zhang F, Del Cardayre SB, Keasling JD. Microbial engineering for the production of advanced biofuels. Nature 2012;488(7411):320–8. https://doi.org/10.1038/nature11478.
[14] Rabinovitch-Deere CA, Oliver JW, Rodriguez GM, Atsumi S. Synthetic biology and metabolic engineering approaches to produce biofuels. Chem Rev 2013;113(7):4611–32. https://doi.org/10.1021/cr300361t.
[15] Straathof AJ. Transformation of biomass into commodity chemicals using enzymes or cells. Chem Rev 2014;114(3):1871–908. https://doi.org/10.1021/cr400309c.
[16] Blakey S, Rye L, Wilson CW. Aviation gas turbine alternative fuels: a review. Proc Combust Inst 2011;33(2):2863–85. https://doi.org/10.1016/j.proci.2010.09.011.
[17] International Air Transport Association. IATA annual reviews. 2017.
[18] ASTM D7566-18. Standard specification for aviation turbine fuel containing synthesized hydrocarbons. West Conshohocken, PA: ASTM International; 2018. https://doi.org/10.1520/D7566-18.
[19] ASTM D7974-15. Standard test method for determination of farnesane, saturated hydrocarbons, and hexahydrofarnesol content of synthesized iso-paraffins (SIP) fuel for blending with jet fuel by gas chromatography. West Conshohocken, PA: ASTM International; 2015. https://doi.org/10.1520/D7974-15.
[20] Chuck CJ, Donnelly J. The compatibility of potential bioderived fuels with Jet A-1 aviation kerosene. Appl Energy 2014;118:83–91. https://doi.org/10.1016/j.apenergy.2013.12.019.
[21] Widegren JA, Bruno TJ. Thermal stability of RP-2 as a function of composition: the effect of linear, branched, and cyclic alkanes. Energy Fuels 2013;27(9):5138–43. https://doi.org/10.1021/ef401677g.
[22] Renninger NS, McPhee DJ. inventor; Amyris Biotechnologies, Inc., assignee. Fuel compositions comprising farnesane and farnesene derivates and method of making and using same. United States patent US 7,399,323. 2008.
[23] Ryder JA. inventor; Amyris Biotechnologies, Inc., assignee. Jet fuel compositions. United States patent US 7,589,243. 2009.
[24] Conconi CC, Crnkovic PM. Thermal behavior of renewable diesel from sugar cane, biodiesel, fossil diesel and their blends. Fuel Process Technol 2013;114:6–11. https://doi.org/10.1016/j.fuproc.2013.03.037.
[25] Won SH, Dooley S, Veloo PS, Wang H, Oehlschlaeger MA, Dryer FL, et al. The combustion properties of 2,6,10-trimethyl dodecane and a chemical functional group analysis. Combust Flame 2014;161(3):826–34. https://doi.org/10.1016/j.combustflame.2013.08.010.
[26] Tekawade A, Oehlschlaeger MA. An experimental study of the spray ignition of alkanes. Fuel 2016;185:381–93. https://doi.org/10.1016/j.fuel.2016.07.108.
[27] Valco DJ, Min K, Oldani A, Edwards T, Lee T. Low temperature autoignition of conventional jet fuels and surrogate jet fuels with targeted properties in a rapid compression machine. Proc Combust Inst 2017;36(3):3687–94. https://doi.org/10.1016/j.proci.2016.05.032.
[28] Millo F, Bensaid S, Fino D, Marcano SJC, Vlachos T, Debnath BK. Influence on the performance and emissions of an automotive Euro 5 diesel engine fueled with F30 from Farnesane. Fuel 2014;138:134–42. https://doi.org/10.1016/j.fuel.2014.07.060.
[29] Oßwald P, Whitside R, Schäffer J, Köhler M. An experimental flow reactor study of the combustion kinetics of terpenoid jet fuel compounds: Farnesane, p-menthane and p-cymene. Fuel 2017;187:43–50. https://doi.org/10.1016/j.fuel.2016.09.035.
[30] Richter S, Kathrotia T, Naumann C, Kick T, Slavinskaya N, Braun-Unkhoff M, et al. Experimental and modeling study of farnesane. Fuel 2018;215:22–9. https://doi.org/10.1016/j.fuel.2017.10.117.
[31] Ji C, Dames E, Wang YL, Wang H, Egolfopoulos FN. Propagation and extinction of premixed C5–C12 n-alkane flames. Combust Flame 2010;157(2):277–87. https://doi.org/10.1016/j.combustflame.2009.06.011.
[32] Fernández-Ramos A, Miller JA, Klippenstein SJ, Truhlar DG. Modeling the kinetics of bimolecular reactions. Chem Rev 2006;106(11):4518–84. https://doi.org/10.1021/cr050205w.
[33] Tsang W. Chemical kinetic data base for combustion chemistry. Part 3: propane. J Phys Chem Ref Data 1988;17(2):887–951. https://doi.org/10.1063/1.555806.
[34] Tsang W. Chemical kinetic data base for combustion chemistry. Part 4. isobutane. J Phys Chem Ref Data 1990;19(1):1–68. https://doi.org/10.1063/1.555877.
[35] Curran HJ, Gaffuri P, Pitz WJ, Westbrook CK. A comprehensive modeling study of n-heptane oxidation. Combust Flame 1998;114(1–2):149–77. https://doi.org/10.1016/S0010-2180(97)00282-4.
[36] Curran HJ, Gaffuri P, Pitz WJ, Westbrook CK. A comprehensive modeling study of iso-octane oxidation. Combust Flame 2002;129(3):253–80. https://doi.org/10.1016/S0010-2180(01)00373-X.
[37] Orme J, Curran H, Simmie J. Experimental and modeling study of methyl cyclohexane pyrolysis and oxidation. J Phys Chem A 2006;110(1):114–31. https://doi.org/10.1021/jp0543678.
[38] Zhang K, Banyon C, Bugler J, Curran HJ, Rodriguez A, Herbinet O, et al. An updated experimental and kinetic modeling study of n-heptane oxidation. Combust Flame 2016;172:116–35. https://doi.org/10.1016/j.combustflame.2016.06.028.
[39] Zhang K, Banyon C, Burke U, Kukkadapu G, Wagnon SW, Mehl M, et al. An experimental and kinetic modeling study of the oxidation of hexane isomers: Developing consistent reaction rate rules for alkanes. Combust Flame 2019;206:123–37. https://doi.org/10.1016/j.combustflame.2019.04.011.
[40] Tsang W, McGivern WS, Manion JA. Multichannel decomposition and isomerization of octyl radicals. Proc Combust Inst 2009;32(1):131–8. https://doi.org/10.1016/j.proci.2008.05.048.
[41] Awan IA, McGivern WS, Tsang W, Manion JA. Decomposition and isomerization of 5-methylhex-1-yl radical. J Phys Chem A 2010;114(30):7832–46. https://doi.org/10.1021/jp102313p.
[42] Ratkiewicz A, Truong TN. Kinetics of the C-C bond beta scission reactions in alkyl radical reaction class. J Phys Chem A 2012;116(25):6643–54. https://doi.org/10.1021/jp3018265.
[43] Blanquart G, Pepiot-Desjardins P, Pitsch H. Chemical mechanism for high temperature combustion of engine relevant fuels with emphasis on soot precursors. Combust Flame 2009;156(3):588–607. https://doi.org/10.1016/j.combustflame.2008.12.007.
[44] Sarathy SM, Westbrook CK, Mehl M, Pitz WJ, Togbe C, Dagaut P, et al. Comprehensive chemical kinetic modeling of the oxidation of 2-methylalkanes from C7 to C20. Combust Flame 2011;158(12):2338–57. https://doi.org/10.1016/j.combustflame.2011.05.007.
[45] Zhao Y, Truhlar DG. The M06 suite of density functionals for main group thermochemistry, thermochemical kinetics, noncovalent interactions, excited states, and transition elements: two new functionals and systematic testing of four M06-class functionals and 12 other function. Theor Chem Acc 2008;120(1–3):215–41. https://doi.org/10.1007/s00214-007-0310-x.
[46] Jiménez-Cruz F, Laredo GC. Molecular size evaluation of linear and branched paraffins from the gasoline pool by DFT quantum chemical calculations. Fuel 2004;83(16):2183–8. https://doi.org/10.1016/j.fuel.2004.06.010.
[47] Dos Santos VML, Da Silva JAB, Stragevitch L, Longo RL. Thermochemistry of biodiesel oxidation reactions: A DFT study. Fuel 2011;90(2):811–7. https://doi.org/10.1016/j.fuel.2010.09.017.
[48] Cardoso DVV, Cunha LA, Spada RFK, Petty CA, Ferrão LFA, Roberto-Neto O, et al. Thermochemical and kinetics of $CH_3SH + H$ reactions: the sensitivity of coupling the low and high-level methodologies. J Phys Chem A 2017;121(2):419–28. https://doi.org/10.1021/acs.jpca.6b09272.
[49] de Carvalho E, Roberto-Neto O. Effects of multidimensional tunneling in the kinetics of hydrogen abstraction reactions of $O(^3P)$ with H_3OCHO. J Comput Chem 2018. https://doi.org/10.1002/jcc.25211.
[50] Xu W, Fan H. Kinetics of reaction RH + O2 = R + HO2 (RH = normal C1–C14 alkanes): a DFT investigation. Fuel 2018;234:1165–72. https://doi.org/10.1016/j.fuel.2018.07.153.
[51] Dunning Jr TH. Gaussian basis sets for use in correlated molecular calculations. I. The atoms boron through neon and hydrogen. J Chem Phys 1989;90(2):1007–23. https://doi.org/10.1063/1.456153.
[52] Papajak E, Truhlar DG. Efficient diffuse basis sets for density functional theory. J Chem Theory Comput 2010;6(3):597–601. https://doi.org/10.1021/ct900566x.
[53] Alecu I, Zheng J, Zhao Y, Truhlar DG. Computational thermochemistry: scale factor databases and scale factors for vibrational frequencies obtained from electronic model chemistries. J Chem Theory Comput 2010;6(9):2872–87. https://doi.org/10.1021/ct100326h.
[54] Frisch MJ, Trucks GW, Schlegel HB, Scuseria GE, Robb MA, Cheeseman JR, et al. Gaussian 09, Revision B.01. Wallingford CT: Gaussian, Inc.; 2010.
[55] Eyring H. The activated complex in chemical reactions. J Chem Phys 1935;3(2):107–15. https://doi.org/10.1063/1.1749604.
[56] Wigner E. Calculation of the rate of elementary association reactions. J Chem Phys 1937;5(9):720–5. https://doi.org/10.1063/1.1750107.
[57] Laidler KJ. The development of the Arrhenius equation. J Chem Educ 1984;61(6):494. https://doi.org/10.1021/ed061p494.
[58] Hindmarsh AC. ODEPACK, a systematized collection of ODE solvers. In: Stepleman

RS, editor. Scientific computing, IMACS transactions on scientific computation. 10th IMACS world congress on systems simulation and scientific computation; 1982 Aug 8–13; Montreal, Canada. Amsterdam: North-Holland; 1983. pp. 55–64.
[59] Radhakrishnan K (Sverdrup Technology Inc, Brook Park, OH), Hindmarsh AC (Lawrence Livermore National Laboratory, Livermore, CA), Description and use of LSODE, the Livermore solver for ordinary differential equations. Cleveland (OH): National Aeronautics and Space Administration, Lewis Research Center; 1993 Dec. Tech. Rep. No.: NASA-RP-1327; UCRL-ID-113855. Contract No: NAS3-25266.
[60] ESI Group. Scilab: Free and open source software for numerical computation, version 6.0.2. Orsey FR: ESI Group; 2019. URL: http://www.scilab.org.
[61] Mzé-Ahmed A, Hadj-Ali K, Dagaut P, Dayma G. Experimental and modeling study of the oxidation kinetics of n-undecane and n-dodecane in a jet-stirred reactor. Energy Fuels 2012;26(7):4253–68. https://doi.org/10.1021/ef300588j.
[62] Vasu SS, Davidson DF, Hong Z, Vasudevan V, Hanson RK. n-dodecane oxidation at high-pressures: measurements of ignition delay times and OH concentration time-histories. Proc Combust Inst 2009;32 I(1):173–180. https://doi.org/10.1016/j.proci.2008.05.006.
[63] Shao J, Choudhary R, Peng Y, Davidson DF, Hanson RK. A shock tube study of n-heptane, iso-octane, n-dodecane and iso-octane/n-dodecane blends oxidation at elevated pressures and intermediate temperatures. Fuel 2019;243:541–53. https://doi.org/10.1016/j.fuel.2019.01.152.